Lakshminarayana, B., 1981, "Techniques for Aerodynamic and Turbulence Measurements in Turbomachinery Rotors," ASME *Journal of Engineering for Power,* Vol. 103, pp. 374–392.

Liu, X., and Rodi, W., 1992, "Measurement of Unsteady Flow and Heat Transfer in a Linear Turbine Cascade," ASME Paper No. 92-GT-323.

Lyman, F. A., 1993, "On the Conservation of Rothalpy in Turbomachines," ASME JOURNAL OF TURBOMACHINERY, Vol. 115, pp. 520–526.

Moore, J., and Moore, J. G., 1993, discussion to the paper "Experimental and Computational Investigation of the NASA Low-Speed Centrifugal Compressor Flow Field," by Hathaway, M. D., Chriss, R. M., Wood, J. R., and Strazisar, A. J., ASME JOURNAL OF TURBOMACHINERY, Vol. 115, pp. 541–542.

Perdichizzi, A., Ubaldi, M., and Zunino, P., 1990, "A Hot Wire Measuring Technique for Mean Velocity and Reynolds Stress Components in Compressible Flow," *Proceedings of the 10th Symposium on Measuring Techniques for Transonic and Supersonic Flows in Cascades and Turbomachines,* VKI, Brussels, Belgium, Paper No. 8.

Pfeil, H., Herbst, R., and Schroeder, T., 1983, "Investigation of the Laminar-Turbulent Transition of Boundary Layers Disturbed by Wakes," ASME *Journal of Engineering for Power,* Vol. 105, pp. 130–137.

Poensgen, C., and Gallus, H. E., 1991a, "Three-Dimensional Wake Decay Inside of a Compressor Cascade and Its Influence on the Downstream Unsteady Flow Field. Part I: Wake Decay Characteristics in the Flow Passage," ASME JOURNAL OF TURBOMACHINERY, Vol. 113, pp. 180–189.

Poensgen, C., and Gallus, H. E., 1991b, "Three-Dimensional Wake Decay Inside of a Compressor Cascade and Its Influence on the Downstream Unsteady Flow Field. Part II: Unsteady Flow Field Downstream of the Stator," ASME JOURNAL OF TURBOMACHINERY, Vol. 113, pp. 190–197.

Schulz, H. D., Gallus, H. E., and Lakshminarayana, B., 1990, "Three-Dimensional Separated Flow Field in the Endwall Region of an Annular Compressor Cascade in the Presence of Rotor-Stator Interaction. Part 2—Unsteady Flow and Pressure Field," ASME JOURNAL OF TURBOMACHINERY, Vol. 112, pp. 679–690.

Suder, K. L., Hathaway, M. D., Okiishi, T. H., Strazisar, A. J., and Adamczyk, J. J., 1987, "Measurements of the Unsteady Flow Field Within the Stator Row of a Transonic Axial-Flow Fan I—Measurement and Analysis Technique," ASME Paper No. 87-GT-226.

Ubaldi, M., Zunino, P., and Cattanei, A., 1993a, "Relative Flow and Turbulence Measurements Downstream of a Backward Centrifugal Impeller," ASME JOURNAL OF TURBOMACHINERY, Vol. 115, pp. 543–551.

Ubaldi, M., Zunino, P., and Cattanei, A., 1993b, "Relative Flow and Turbulence Measurements Downstream of an Axial Flow Rotor," *Engineering Turbulence Modelling and Experiments 2,* W. Rodi and F. Martelli, eds., Elsevier Science Pub., pp. 795–804.

Zeschky, J., and Gallus, H. E., 1993, "Effects of Stator Wakes and Spanwise Nonuniform Inlet Conditions on the Rotor Flow of an Axial Turbine Stage," ASME JOURNAL OF TURBOMACHINERY, Vol. 115, pp. 128–136.

Zierke, W. C., and Okiishi, T. H., 1982, "Measurement and Analysis of Total-Pressure Unsteadiness Data From an Axial-Flow Compressor Stage," ASME *Journal of Engineering for Power,* Vol. 104, pp. 479–488.

APPENDIX

Diffuser Vane Profile Geometry

The diffuser vanes are thin constant thickness circular arc aerofoils. The geometry is defined by the following parameters:

- Radius of curvature of the camber line R_c = 332 mm.
- Angle between the camber line chord and the radial direction at the inlet $\lambda_{3'}$ = 101.65 deg.
- Inlet and outlet radii of the camber line $R_{3'}$ = 223.94 mm, R_4 = 332 mm.
- Constant thickness of the profile 8 mm.

Reduced thickness at the leading edge 4 mm, obtained by a linear cut of the airfoil on the pressure side from 13 percent of the camber line to the leading edge.

Impeller blade profile coordinates

Suction side		Pressure side	
R (mm)	θ (deg)	R (mm)	θ (deg)
120.00	0.00	120.00	0.00
120.48	1.61	122.76	1.16
121.06	3.21	124.91	2.79
121.74	4.79	126.76	4.10
122.50	6.36	128.71	5.40
123.36	7.91	130.77	6.69
124.31	9.43	132.95	7.96
128.31	13.62	137.43	11.86
132.58	17.67	141.73	15.98
136.86	21.65	146.03	20.04
141.13	25.60	150.33	24.05
145.40	29.50	154.63	28.03
149.67	33.37	158.92	31.96
153.94	37.21	163.22	35.86
158.22	41.01	167.52	39.72
162.49	44.79	171.81	43.54
166.77	48.52	176.11	47.33
171.05	52.22	180.40	51.06
175.33	55.87	184.69	54.75
179.61	59.47	188.98	58.39
183.89	63.02	193.27	61.97
188.17	66.52	197.56	65.49
192.45	69.95	201.85	68.95
196.74	73.31	206.13	72.34
201.02	76.61	210.42	75.66
203.83	77.59	210.34	77.00
206.67	78.52	210.36	78.23
209.53	79.42	210.47	79.33

DISCUSSION

Y. N. Chen[1]

The authors of the paper have presented very useful informations about the flow fields due to interaction between the impeller blades and the diffuser vanes.

The present discusser has discovered a special phenomenon of the secondary flow field, which may be of interest to the authors. The secondary flow field displayed in the lowest plot of Fig. 6 reveals a secondary vortex embedded just in the region, in which the throughflow momentum wake appears; see the upper plot of the same figure. This secondary vortex field is indicated by a circular curve L in Fig. 14(b).

The authors explained that the throughflow momentum wake is caused by the tip leakage action, which produces losses and convects them toward the pressure side.

However, if the secondary flow field mentioned is closely examined, the leakage flow of the tip clearance does not have any connection with this secondary vortex. Rather, this leakage flow meets the further secondary flow traveling in the opposite direction along the shroud. The meeting region of these two flows, as denoted by S in Fig. 14(b), must be a sink. As this region is situated within the dark area of the throughflow in the upper plot of Fig. 6, i.e., thus within the area of the lowest velocity, this sink therefore appears to guide the meeting flows in the reverse direction into the impeller. We then have a reverse flow along the corner "suction-surface/shroud" even at the normal operating point. This kind of reverse flow has been found by Chen et al. (1989) in their Fig. 5.

The upper plot of Fig. 5 of the present paper about the averaged total relative velocity (as transferred to Fig. 14a) shows that the curve rises to a peak along the pressure side of the impeller blade (cf. Fig. 8 about the tangential velocity component alone), drops sharply along the suction side to a minimum of the wake deficit. Afterward, the curve rises toward the pressure surface of the following impeller blade. This rising-up branch does not follow a uniform trend according to the potential theory, but rather a going-up and down pattern. The valley of this pattern is the throughflow momentum wake (as given in the upper plot of Fig. 6), which coincides with the secondary

[1] R & D, 1510, Sulzer Brothers Ltd., 8401 Winterthur, Switzerland.

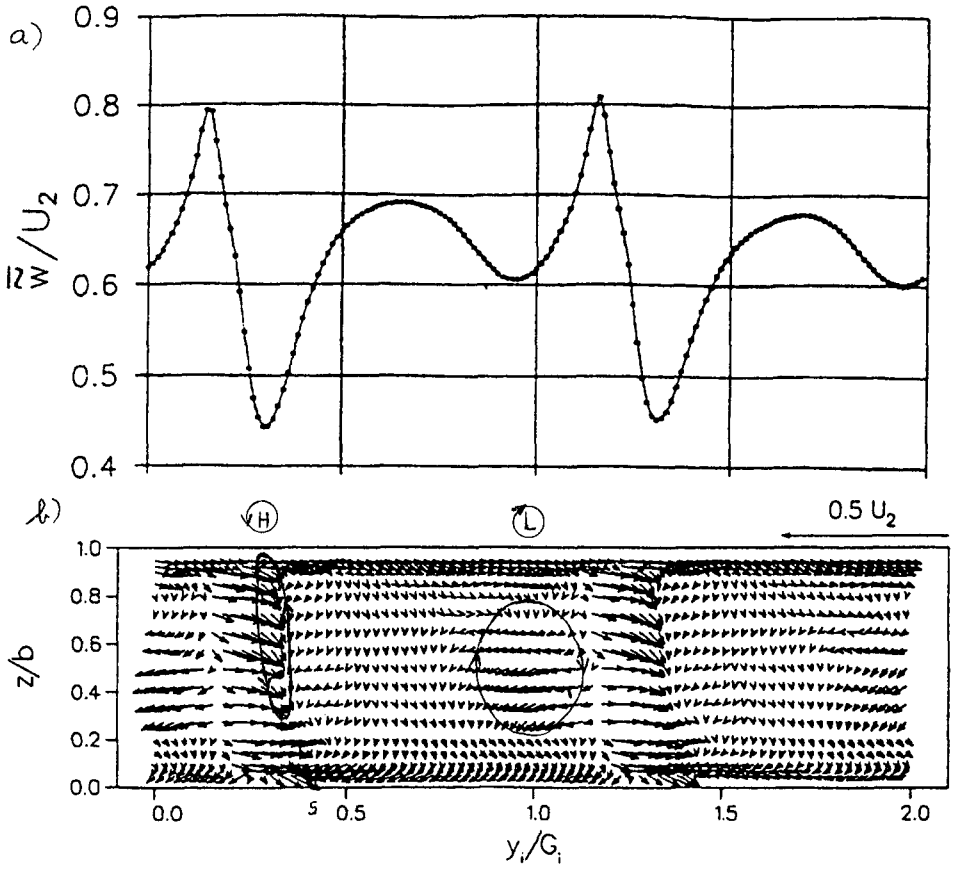

Fig. 14

vortex constructed in Fig. 14(*b*). Thus, this throughflow momentum wake is the core region of the secondary vortex. Only because the wake is protected by the vortex can it exist in the surroundings of the high velocities within the flow field of the blade channel of the impeller. The turbulence level therefore rises to a flat peak in this vortex region (see the lowest plot in Fig. 5).

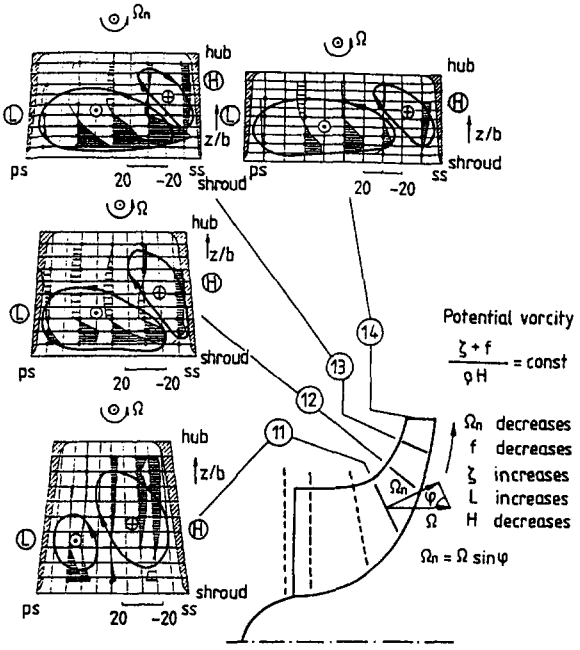

Fig. 15 Secondary flows over the cross sections of a back-swept impeller, normal component of the angular velocity $\Omega_n = \Omega \sin \varphi$

Furthermore, if the secondary flow field in Fig. 14(*b*) is compared with the total-relative-velocity field in Fig. 14(*a*), the secondary flow field is divided by the trailing edge of the impeller blade into two regions: The one on the pressure side is deflected to the left and the other one on the suction side is deflected to the right. The deflection is the strongest in the region of the corner "suction-surface/hub," so that a secondary vortex *H* can be constructed. It is associated with a high throughflow as shown in the upper plot of Fig. 6. This secondary vortex has an opposite rotating sense compared to that of the throughflow momentum wake *L*.

Chen et al. (1991) have considered the secondary vortices in the blade channel as the developing Dean's type vortices of the curvature of the impeller. If the cross section No. 11 of the curvature in Fig. 15 is considered, the normal component Ω_n of the angular velocity Ω of the rotating axis acting on the cross section causes the secondary flow distributed over this section to rotate accordingly. The Dean vortex pair can be detected from the experimental data of Eckardt and Krain (1977), and Krain (1984) about the secondary flow field on a backswept impeller (Fig. 15). This vortex pair consists of a vortex "low (*L*)," rotating in the sense of Ω_n, and a vortex "high (*H*)," rotating against this sense.

The vortex "low" causes a radial flow toward its core (with the vortex stretching), which is familiar to the cyclone as a low in the atmosphere. This radial flow is then deflected into the axial direction and streams out of the core as an axial flow due to continuity law. The axial flow of the cyclone is directed upward from the high-pressure layer on the ground toward the low-pressure layer of the upper atmosphere. The axial flow of the vortex "low" of the impeller will thus also be directed

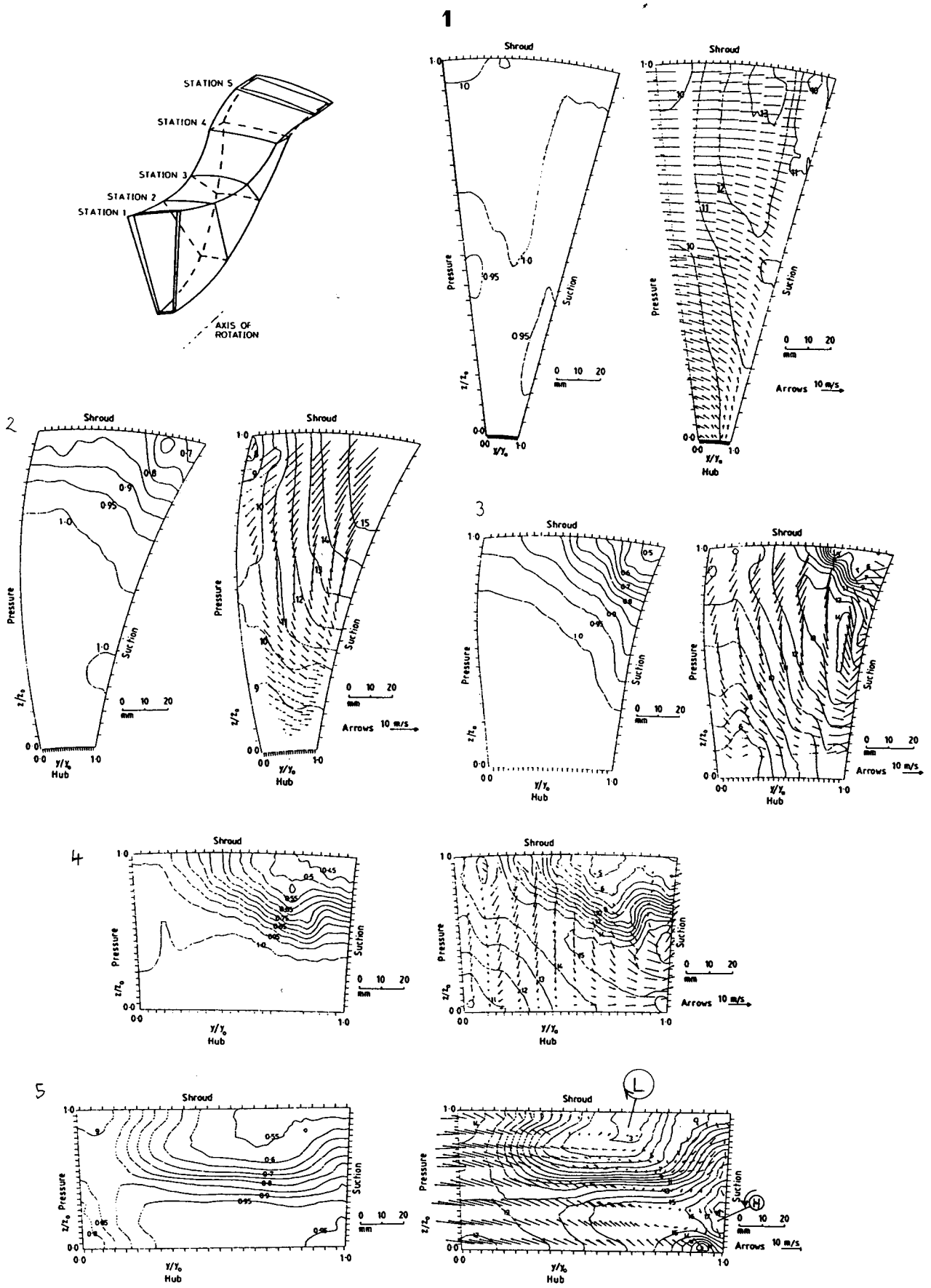

Fig. 16 Secondary flow fields across the sections of the blade channel at five stations, accompanied by the dimensionless rotary stagnation pressure (left diagram) and relative velocity contours in m/s (right diagram)

from its high-pressure layer of the outlet toward its low-pressure layer of the inlet. This axial flow is then a secondary backflow superimposed on the mean flow field: We have a strong throughflow momentum wake in the core region of the vortex "low."

The vortex "high" is associated with a radial flow out of the core, the same as the anticyclone. The axial flow through the core is directed from the low-pressure layer of the upper atmosphere toward the high-pressure layer on the ground. For the case of the impeller, this radial flow will come from the inlet through the core of the vortex "high" toward the outlet and spread out of it. We then have here a strong throughflow momentum jet along of the vortex "high" superimposed on the mean flow field.

The local Coriolis parameter $f = 2\,\Omega_n$ of the secondary flow over the cross section of the impeller-blade channel decreases downstream along the blade channel, while the pressure p increases at the same time.

According to the conservation law of the potential vorticity:

$$\Pi = \frac{\xi + f}{\rho H} = \frac{\xi + f}{p} = \text{const}$$

(Pedlosky, 1984), the relative vorticity ξ in the secondary flow will increase in this downstream direction. This indicates that the secondary vortex "low L" (with a positive sign of ξ) will strengthen and the secondary vortex "high H" (with a negative sign of ξ) will diminish along the blade channel in this downstream direction.

The derivation given above is verified by the experimental result given in Fig. 15 (Chen et al., 1991). The secondary vortex pair develops from the section 11 to the section 14 (i.e., the outlet) with the result that the vortex "low L" in the corner "pressure/shroud" becomes very huge in the outlet section 14, while the vortex "high H" in the corner "suction/hub" diminishes to a small intensity.

A further experimental result about the secondary flow of a backswept impeller obtained by Farge and Johnson (1990) is given in Fig. 16 along the blade channel in five stations. Each station consists of the secondary flows, in addition to the contours of the throughflow velocities (in the right diagram) and the dimensionless rotary stagnation pressure (in the left diagram).

At station 1 for the inlet of the blade channel, a passage vortex rotating against the rotational sense of the impeller forms the field of the secondary flow. This passage vortex keeps the absolute vorticity of the secondary flow at the zero value, because the throughflow has originated from the absolute frame with zero vorticity. This passage vortex is thus a huge "high H." The corresponding rotary stagnation pressure remains high at 0.95 to 1 with a very uniform distribution across the section of the inlet.

This very regular passage vortex then degenerates with the throughflow traveling downstream: A low-pressure center of 0.7 near the corner "section/shroud" at station 2, followed by 0.5 and 0.45 at stations 3 and 4, respectively. The low-pressure center of 0.55 becomes very broad at station 5, i.e., at the outlet section of the impeller, while the high-pressure center of 0.95 reduces to a smaller size in the corner region of the "suction/hub." The corresponding secondary velocity field is quite similar to that in Fig. 15.

The difference in the arrangements of the vortex pairs in the two experiments given in Figs. 15 and 16 is caused by the different shapes of the blade channels investigated. Thus these two experiments bear the evidence for the validity of the conservation of the potential vorticity along the blade channel.

The secondary vortices L and H in Fig. 14(b) correspond very well to those given in Figs. 15 and 16 over the outlet section of the impeller. Then, the vortex L is a pressure "low" centered on the throughflow momentum wake and the vortex H is a pressure "high" centered on the throughflow momentum jet, as given in Fig. 6.

References

Chen, Y. N., Haupt, U., and Rautenberg, M., 1989, "The Vortex-Filament Nature of Reverse Flow on the Verge of Rotating Stall," ASME JOURNAL OF TURBOMACHINERY, Vol. 111, pp. 450–461.

Chen, Y. N., Seidel, U., Haupt, U., and Rautenberg, M., 1991, "The Rossby Waves of Rotating Stall in Impellers, Part II: Application of the Rossby-Wave Theory to Rotating Stall," *Proceedings, 1991 Yokohama International Gas Turbine Congress,* pp. I/77–88.

Eckardt, D., and Krain, H., 1977, "Secondary Flow Studies in High-Speed Centrifugal Impellers," AGARD Conference "Secondary Flows in Turbomachines," Den Haag, AGARD CP 214, pp. 18/1–13.

Farge, T. Z., and Johnson, M. W., 1990, "The Effect of Backswept Blading on the Flow in a Centrifugal Compressor Impeller," ASME Paper No. 90-GT-231.

Krain, H., 1984., "Experimental Observation of the Flow in Impellers and the Diffusers," Lecture 1984-07, "Flow in Centrifugal Compressors," von Karman Institute for Fluid Dynamics.

Pedlosky, J., 1984, *Geophysical Fluid Dynamics,* Springer-Verlag, New York–Berlin–Heidelberg–Tokyo.

Authors' Closure

The authors wish to thank Dr. Chen for the comment and the kind attention to the results shown in the paper.

Dr. Chen has developed an original theory based on the analogy between geophysical and turbomachinery flows, which is useful to help interpret the complex secondary flow pattern in centrifugal turbomachinery rotors. Most secondary flow fields seem to be explainable in terms of a pair of counterrotating vortices, which verify the conservation law of the potential vorticity. The two vortices generate flow along their axis: One against the primary flow gives rise to the throughflow wake, the second in the opposite direction determines a momentum jet superimposed on the main flow field.

Compared with the cases mentioned in the discussion, the present impeller geometry represents a limiting case, as the blades are set in the wholly radial part of the meridional channel. In this case the component of the rotational speed vector normal to the inlet cross section tends to zero and therefore should not be responsible for the "low" vortex identified by Dr. Chen in the secondary flow field.

It is the authors' opinion that the position and the intensity of the low-momentum throughflow wake are strongly determined in the unshrouded impellers by the tip clearance effects. Evidence of that can be found in the experimental results and numerical predictions of Hathaway et al. (1993), in the computational investigation of Moore and Moore (1993) performed on the same impeller, without tip clearance and with different tip clearance gaps, and in the experimental data and computations of Hah and Krain (1990).

The authors are more familiar with secondary flow explanation based on the equilibrium of the fluid dynamic forces in the relative frame of reference and on the unbalance due to the presence of boundary layers near blades and endwall surfaces or to the tip clearance. However, they think that the two approaches are complementary and that the use of both may allow a more refined analysis and better understanding of the phenomena.

References

Hah, C., and Krain, H., 1990, "Secondary Flows and Vortex Motion in a High-Efficiency Backswept Impeller at Design and Off-Design Conditions," ASME JOURNAL OF TURBOMACHINERY, Vol. 112, pp. 7–13.